J. KSIAM Vol.14, No.4, 201–210, 2010

A FAST AND ACCURATE NUMERICAL METHOD FOR MEDICAL IMAGE SEGMENTATION

YIBAO LI AND JUNSEOK KIM†

DEPARTMENT OF MATHEMATICS, KOREA UNIVERSITY, SEOUL 136-701, REPUBLIC OF KOREA
E-mail address: cfdkim@korea.ac.kr

ABSTRACT. We propose a new robust and accurate method for the numerical solution of medical image segmentation. The modified Allen-Cahn equation is used to model the boundaries of the image regions. Its numerical algorithm is based on operator splitting techniques. In the first step of the splitting scheme, we implicitly solve the heat equation with the variable diffusive coefficient and a source term. Then, in the second step, using a closed-form solution for the nonlinear equation, we get an analytic solution. We overcome the time step constraint associated with most numerical implementations of geometric active contours. We demonstrate performance of the proposed image segmentation algorithm on several artificial as well as real image examples.

1. INTRODUCTION

Image segmentation is one of the fundamental tasks in automatic image analysis. Its goal is to partition a given image into several regions in each of which the intensity is homogeneous. Up to now, a great number of algorithms have been proposed to solve the image segmentation problem. Among them, there are two widely used classical basic models based on the edges or the regions. For the geodesic snake based on the edges [2, 4, 5, 8, 9, 13], a gradient flow is used as a stopping operator to get accurate boundaries with high variation in gradient to attract the curve to the object boundary, while Chan-Vese method [6, 12], which is a representative model based on the regions, is widely applied for various applications in image processing applications. We are interested in medical image segmentation which has edges, therefore, it is natural choice to use geometric active contour models.

In this paper, we propose a robust and accurate geometric active contour model and its numerical solution algorithm for image segmentation. The model is based on the modified Allen-Cahn equation. The Allen-Cahn (AC) equation was originally introduced as a phenomenological model for anti-phase domain coarsening in a binary alloy [1]. Also, AC equation is used to model mean-curvature flow problems. The mean-curvature flow is one of important ingredients in image segmenting active contours. The main reason why we use AC equation for image segmentation is that there exists a very fast computational technique such as a multigrid method.

Received by the editors July 19 2010; Accepted August 9 2010.
2000 *Mathematics Subject Classification.* 68U10, 65M55.
Key words and phrases. image segmentation, Allen-Cahn equation, phase-field method.
† Corresponding author.

An operator splitting technique is used to solve the model numerically. The nonlinear part in the equation can be solved analytically because there is a closed-form solution. In particular, we propose an initialization algorithm based on an edge stopping function for the fast image segmentation. We present various numerical results on artificial and real images to demonstrate the robustness and the accuracy of the proposed numerical method.

The outline of this paper is the following. In Sec. 2, the governing equation based on Allen-Cahn equation is presented. In Sec. 3, we describe the proposed hybrid operator splitting method. In Sec. 4, we perform some characteristic numerical experiments for computational examples. Finally, conclusions are drawn in Sec. 5.

2. MODIFIED ALLEN-CAHN EQUATION

For a given image $f_0(\mathbf{x})$, where $\mathbf{x} = (x, y)$, on the image domain Ω and its segmenting curve C. By the level-set function $\phi(\mathbf{x})$,

$$\phi(\mathbf{x}) \begin{cases} > 0 & \text{if } \mathbf{x} \in \text{inside } C, \\ = 0 & \text{if } \mathbf{x} \in C, \\ < 0 & \text{if } \mathbf{x} \in \text{outside } C. \end{cases}$$

The geometric active contour model based on the mean curvature motion is given by the following evolution equation [4]:

$$\phi_t = g(f_0)|\nabla\phi|\nabla\cdot\left(\frac{\nabla\phi}{|\nabla\phi|}\right) + \lambda g(f_0)|\nabla\phi|,$$

where λ is a parameter and g is an edge stopping function. For example,

$$g(f_0(\mathbf{x})) = \frac{1}{1+|\nabla(G_\sigma * f_0)(\mathbf{x})|^k}, \tag{2.1}$$

where we will use $k = 2$ and $(G_\sigma * f_0)(\mathbf{x})$, a smoother version of f_0, is the convolution of the given image f_0 with the Gaussian function $G_\sigma = \frac{1}{2\pi\sigma^2}e^{-(x^2+y^2)/(2\sigma^2)}$. The function $g(f_0(\mathbf{x}))$ is close to zero where the gradient of the image is high and is close to one in homogeneous regions.

We propose a phase-field approximation for the geometric active segmentation by using the modified Allen-Cahn equation. In a phase-field model, we introduce a phase-field, ϕ, which is plus one (black) and minus one (white). Then, the governing equation is as follows:

$$\phi_t = g(f_0)\left(-\frac{F'(\phi)}{\epsilon^2} + \Delta\phi\right) + \lambda g(f_0)F(\phi), \tag{2.2}$$

where $F(\phi) = 0.25(1-\phi^2)^2$ is a double-well potential. Note that Eq. (2.2) is similar to the model proposed in [3], however, the new one is more robust and efficient than the previous model.

In Eq. (2.2), $g(f_0)$ is an edge stopping function which makes the evolution of the phase-field slow. $\phi_t = -\frac{F'(\phi)}{\epsilon^2} + \Delta\phi$ is the equation for the motion by mean curvature. Depending on the sign of λ, $\lambda F(\phi)$ makes the level set of the phase-field grows or shrinks.

3. PROPOSED NUMERICAL SOLUTION

In this section, we shall discretize Eq. (2.2) in a two dimensional space, i.e., $\Omega = (a,b) \times (c,d)$. Let N_x and N_y be positive even integers, $\Delta x = (b-a)/N_x$, $\Delta y = (d-c)/N_y$ be the uniform mesh sizes. For simplicity of exposition, we take $\Delta x = \Delta y = h$. Let $\Omega_h = \{(x_i, y_j) : x_i = (i-0.5)h,\ y_j = (j-0.5)h,\ 1 \le i \le N_x,\ 1 \le j \le N_y\}$ be the set of cell centers. Let ϕ_{ij}^n be approximations of $\phi(x_i, y_j, n\Delta t)$, where Δt is the time step. The numerical convolution $G_\sigma * f_0$ can be computed using a 3×3 smoothing kernel as following:

$$(G_\sigma * f_0)_{ij} = \sum_{p=i-1}^{i+1} \sum_{q=j-1}^{j+1} \frac{f_{0pq}}{2\pi\sigma^2} e^{-\frac{[(i-p)^2+(j-q)^2]h^2}{2\sigma^2}}.$$

Then, the edge function can be calculated by

$$g(f_0)_{ij} = \frac{1}{1 + (G_\sigma * f_0)_{x,ij}^2 + (G_\sigma * f_0)_{y,ij}^2},$$

where $(G_\sigma * f_0)_{x,ij} = [(G_\sigma * f_0)_{i+1,j} - (G_\sigma * f_0)_{i-1,j}]/(2h)$. The zero Neumann boundary condition is used. For example, $f_{0N_x+1,j} = f_{0N_x,j}$ for $j = 1, \cdots, N_y$. Then we propose the following operator splitting numerical algorithm for Eq. (2.2):

$$\frac{\phi_{ij}^* - \phi_{ij}^n}{\Delta t} = g_{ij}\Delta_d \phi_{ij}^* + \lambda g_{ij} F(\phi_{ij}^n), \tag{3.1}$$

$$\frac{\phi_{ij}^{n+1} - \phi_{ij}^*}{\Delta t} = -g_{ij}\frac{F'(\phi_{ij}^{n+1})}{\epsilon^2}, \tag{3.2}$$

If we add these two equations, then we have

$$\frac{\phi_{ij}^{n+1} - \phi_{ij}^n}{\Delta t} = g_{ij}\left(-\frac{F'(\phi_{ij}^{n+1})}{\epsilon^2} + \Delta_d \phi_{ij}^*\right) + \lambda g_{ij} F(\phi_{ij}^n). \tag{3.3}$$

The implicit discrete Eq. (3.1) can be solved by a multigrid method [11] with the initial condition ϕ^n. Since we can consider Eq. (3.2) as an approximation of the equation

$$\phi_t = g\frac{\phi - \phi^3}{\epsilon^2} \tag{3.4}$$

by an implicit Euler's method with the initial condition ϕ^*. Then the solution at $t = \Delta t$ of Eq. (3.4), solved by the method of separation of variables [10], is given as

$$\phi_{ij}^{n+1} = \frac{\phi_{ij}^*}{\sqrt{e^{-\frac{2g_{ij}\Delta t}{\epsilon^2}} + (\phi_{ij}^*)^2\left(1 - e^{-\frac{2g_{ij}\Delta t}{\epsilon^2}}\right)}}.$$

Finally, our proposed scheme is written as

$$\begin{aligned}\frac{\phi_{ij}^{*}-\phi_{ij}^{n}}{\Delta t} &= g_{ij}\Delta_d\phi_{ij}^{*}+\lambda g_{ij}F(\phi_{ij}^{n}),\\ \phi_{ij}^{n+1} &= \frac{\phi_{ij}^{*}}{\sqrt{e^{-\frac{2g_{ij}\Delta t}{\epsilon^2}}+(\phi_{ij}^{*})^2\left(1-e^{-\frac{2g_{ij}\Delta t}{\epsilon^2}}\right)}}.\end{aligned}$$

4. COMPUTATIONAL EXAMPLES

In this section, we present numerical results using the proposed numerical algorithm on various synthetic and real images. We show that a very fast and accurate minimization can be achieved by the proposed algorithm. In our numerical experiments, we normalize the given image f as $f_0 = \frac{f-f_{min}}{f_{max}-f_{min}}$, where f_{max} and f_{min} are the maximum and the minimum values of the given image, respectively. Across the interfacial regions, the phase-field varies from -0.9 to 0.9 over a distance of approximately $2\sqrt{2}\epsilon\tanh^{-1}(0.9)$. Therefore, if we want this value to be approximately m grid points, then the ϵ value needs to be taken as follows:

$$\epsilon_m = \frac{hm}{2\sqrt{2}\tanh^{-1}(0.9)}.$$

The value of m should be at least two or three so that the interface under goes smooth transition, otherwise we will overestimate the discrete Laplacian in the governing equation (2.2). When we have enough number of mesh points, we can afford to use larger value of m so that we have smooth transition in the interfacial region. However, at the same time, we do not want too much smoothed interfacial transitions. To speed up simulation, we simply initialize ϕ^0 with an edge stopping function, g and a given tolerance, tol. The initialization algorithm is listed as follows:

Set a tolerance tol and $\phi^0 = -1$ everywhere in the computational domain. And take the following steps (1–4):

Step 1 for (i=1; $i \le N_x$; i++) for (j=N_y; $j \ge 1$; j- -) {
if ($g_{ij} < tol$) break ; else $\phi_{ij}^0 = 1$;}

Step 2 for (j=1; $j \le N_y$; j++) for (i=1; $i \le N_x$; i++) {
if ($g_{ij} < tol$) break ; else $\phi_{ij}^0 = 1$;}

Step 3 for (i=1; $i \le N_x$; i++) for (j=1; $j \le N_y$; j++) {
if ($g_{ij} < tol$) break ; else $\phi_{ij}^0 = 1$;}

Step 4 for (j=1; $j \le N_y$; j++) for (i=N_x; $i \ge 1$; i- -) {
if ($g_{ij} < tol$) break ; else $\phi_{ij}^0 = 1$;}

In our first example, we show that our proposed model can detect different objects. In Fig. 1, we show how our proposed initialization algorithm works. (a) is the given image and (b), (c), (d), and (e) are steps 1, 2, 3, and 4 in the initialization algorithm, respectively. In Fig. 2, the computational domain is set to $\Omega = (0,1) \times (0,1)$ with a 64×64 mesh. Interface parameter ϵ_4, time step $\Delta t = 4\text{E-}4$, and $\lambda = 1\text{E}4$ are used. It only took 9 iterations, which is one order of magnitude smaller than the method in [8].

(a) (b) (c) (d) (e)

FIGURE 1. Initialization algorithm: (a) original image, (b) Step 1, (c) Step 2, (d) Step 3, and (e) Step 4.

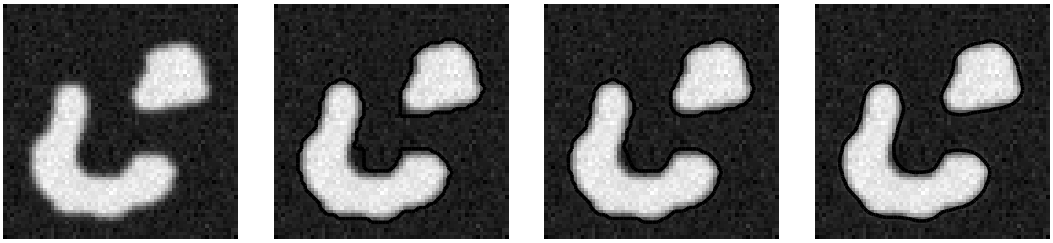

(a) (b) (c) (d)

FIGURE 2. (a) Original image, (b) 0 iteration, (c) 3 iterations, and (d) 9 iterations.

Fig. 3 shows our proposed method is faster than the previous method, which also used the Allen-Cahn equation for image segmentation [3]. The computational domain is set to $\Omega = (0,1) \times (0,1)$ with a 128×128 mesh. Interface parameter ϵ_8, time step $\Delta t = 6\text{E-}4$, and $\lambda = 2.5\text{E}4$ are used. It took only 20 iterations, which is one order of magnitude smaller than the previous method, which used 532 iterations. Here, we also note that without our proposed initialization algorithm, it took 85 iterations in our computational experiment.

Next example image is from [7] and has varying illumination and highly concave shape (see Fig. 4 (a)). The computational domain is set to $\Omega = (0,1) \times (0,1)$ with a 128×128 mesh. Interface parameter ϵ_8, time step $\Delta t = 3\text{E-}4$, and $\lambda = 2\text{E}4$ are used. Fig. 4 (b) shows the initial configuration using our proposed initialization algorithm. As can be seen from Fig. 4 (d), image segmentation is successfully done only after 10 iterations.

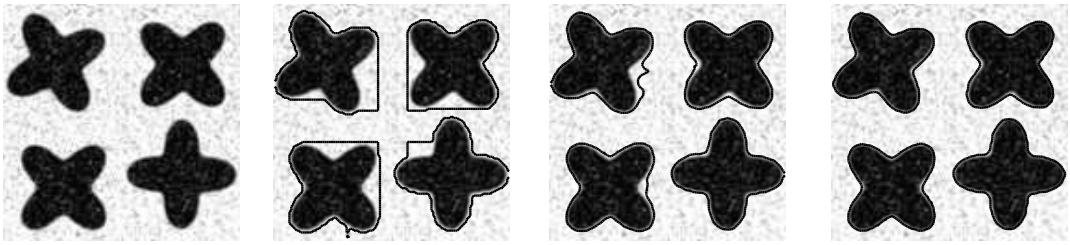

(a) (b) (c) (d)

FIGURE 3. (a) Original image, (b) 0 iteration, (c) 8 iterations, and (d) 20 iterations.

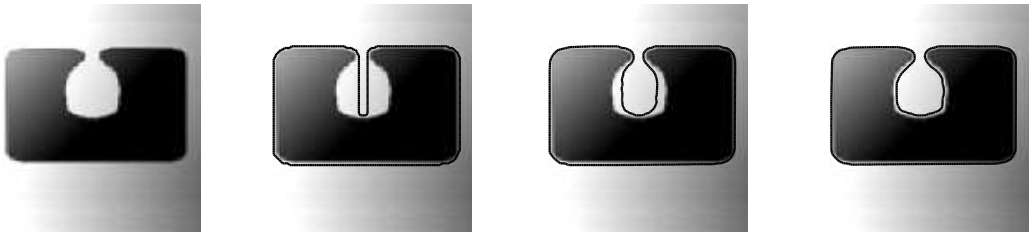

(a) (b) (c) (d)

FIGURE 4. (a) Image which has varying illumination and highly concave shape, (b) 0 iteration, (c) 5 iterations, and (d) 10 iterations.

In Fig. 5, we show a numerical result on a real medical image of a hip joint. The computational domain is set to $\Omega = (0,1) \times (0,1)$ with a 128×128 mesh. Interface parameter ϵ_8, time step $\Delta t =$ 3E-5, and $\lambda =$ 2.5E4 are used. The method produces visually clear results with only 10 iterations. As can be seen, our proposed method has performed well in this medical image segmentation.

In Fig. 6, the segmentation of another hip joint image is shown on the computational domain $\Omega = (0,1) \times (0,1)$ with a 256×256 mesh. Interface parameter ϵ_8, time step $\Delta t =$ 5E-5, and $\lambda =$ 1.5E4 are used. As can be observed, the agreement between the area of hip and the segmentation of image is obvious.

Finally, we will explain why we chose $k = 2$ in Eq. (2.1) by using a synthetic image as shown in Fig. 7(a). This experiment is performed on the computational domain $\Omega = (0,1) \times (0,1)$ with a 128×128 mesh. Interface parameter ϵ_4, time step $\Delta t =$ 5E-5, and $\lambda =$ 5E4 are used. We use the following function as an original image:

$$f(x,y) = \tanh \frac{0.2 - \sqrt{(x-0.5)^2 + (y-0.5)^2}}{\sqrt{2}\epsilon}.$$

Fig. 7(b) shows the edge stopping function, $g(f_0)$, with $k = 1$. As can be observed in Fig. 7(c), when $k = 1$ (solid line), the edge stopping function is not close to zero near the edge

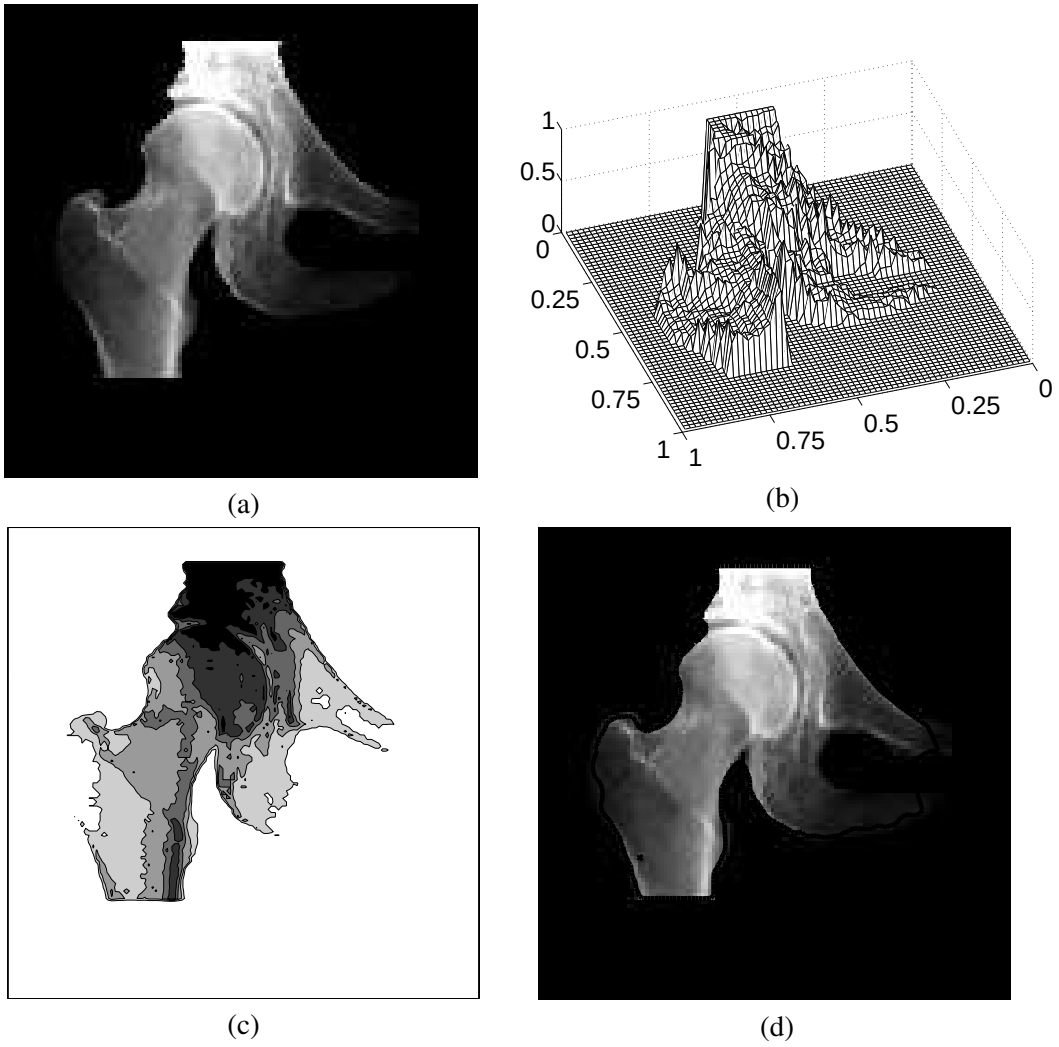

FIGURE 5. (a) Original image, (b) mesh image, (c) contour image, and (d) 10 iterations.

of the image. This implies that the segmenting boundary will evolve toward inside the object boundary we want to segment. Fig. 7(d) shows the numerical result with $k = 1$ and as we expected the segmenting boundary passed the edge of the object at 150 iterations. In the cases of $k = 2$ and 3, the edge stopping functions have almost zero values near the interface. Figs. 7(e) and 7(f) show results with $k = 2$ and $k = 3$, respectively. The segmenting boundary stopped near the edge of the object. Generally, the higher order of k, the costly computational time. Therefore, in practice, $k = 2$ is commonly used.

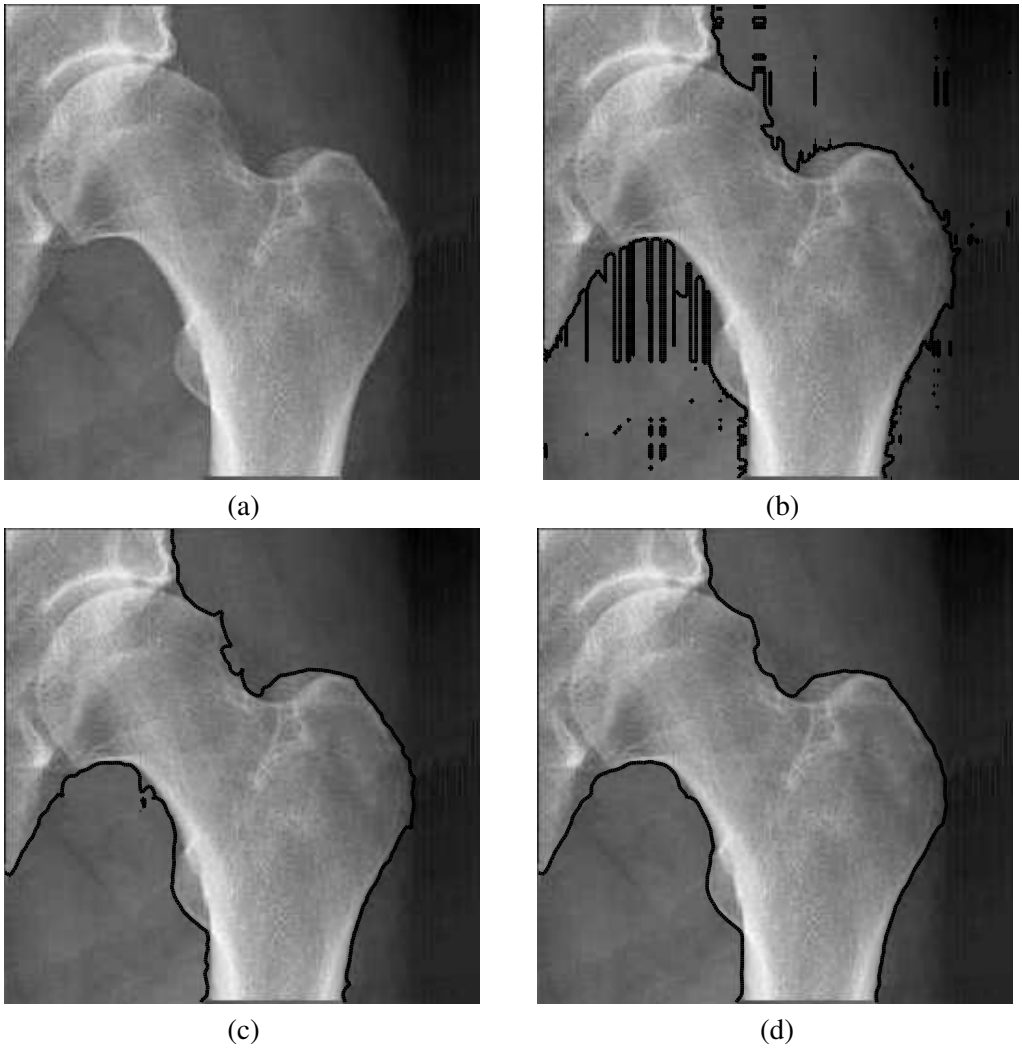

FIGURE 6. (a) Original image, (b) 0 iteration, (c) 4 iterations, and (d) 20 iterations.

5. CONCLUSION

We have shown that our proposed algorithm achieves faster segmentation of binary images than the previous methods. We used a fast solver such as a multigrid method for solving heat equation and an analytic solution for the nonlinear equation. To speed up image segmentation, we developed the initialization algorithm which initialized ϕ^0 with an edge stopping function, g and a given tolerance, tol. We validated the proposed numerical method by various numerical results on artificial and real images.

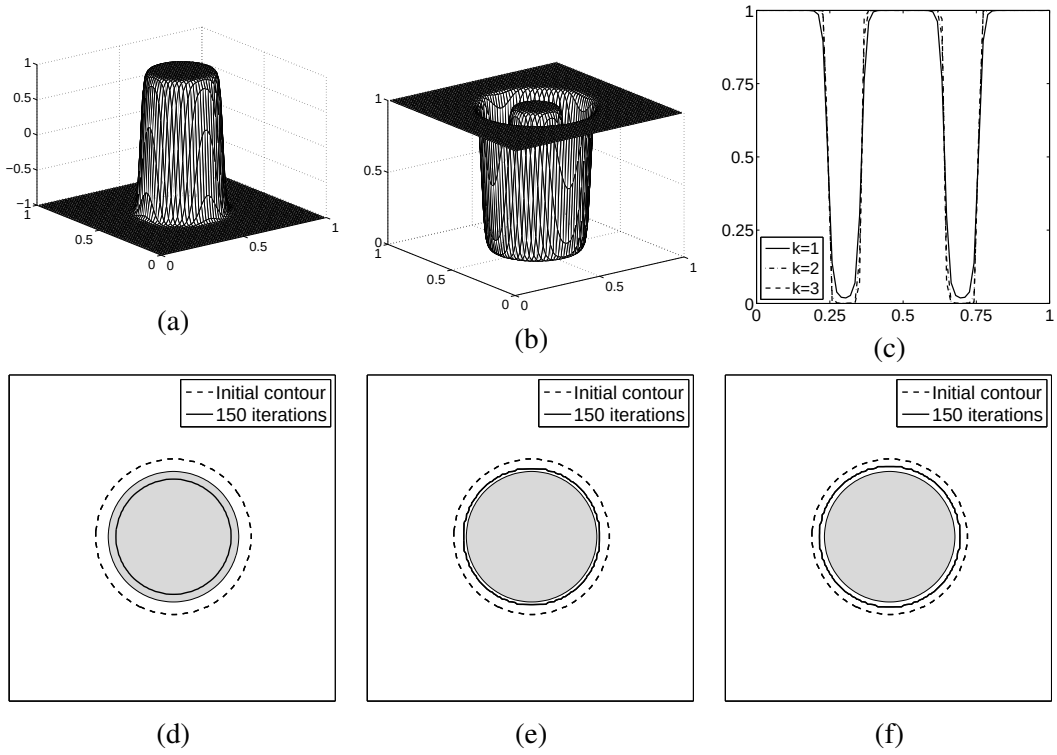

FIGURE 7. (a) Original image, (b) edge stopping function with $k = 1$, (c) slice plot of edge functions at $y = 0.5$ with different k, and (d), (e), and (f) are result contours at 150 iterations with $k = 1$, $k = 2$, and $k = 3$, respectively.

ACKNOWLEDGMENTS

This research was supported by Basic Science Research Program through the National Research Foundation of Korea(NRF) funded by the Ministry of Education, Science and Technology(No. 2009-0074248). The authors also thank the reviewers for the constructive and helpful comments on the revision of this article.

REFERENCES

[1] S.M. Allen and J.W. Cahn, *A microscopic theory for antiphase boundary motion and its application to antiphase domain coarsening*, Acta Metallurgica, **27** (1979), 1085–1095.

[2] B. Appleton and H. Talbot, *Globally optimal geodesic active contours*, Journal of Mathematical Imaging and Vision, **23** (2005), 67-86.

[3] M. Beneš, V. Chalupecký, and K. Mikula, *Geometrical image segmentation by the Allen-Cahn equation*, Applied Numerical Mathematics, **51** (2-3) (2004), 187–205.

[4] V. Caselles, F. Catte, T. Coll, and F. Dibos, *A geometric model for active contours in image processing*, Numerische Mathematik, **66** (1993), 1–31.

[5] V. Caselles, R. Kimmel, and G. Sapiro, *Geodesic active contours*, International Journal of Computer Vision, **22** (1) (1997), 61–79.
[6] T. Chan and L. Vese, *Active contours without edges*, IEEE Transactions on image processing, **10** (2) (2001), 266–277.
[7] J. Hahn and C-O. Lee, *Geometric attraction-driven flow for image segmentation and boundary detection*, Journal of Visual Communication and Image Image Representation, **21** (2010), 56-66.
[8] C. Li, C. Xu, C. Gu, and M.D. Fox, *Level set evolution without re-initialization: a new variational formulation*, IEEE International Conference on Computer Vision and Pattern Recognition, San Diego, (2005), 430–436.
[9] S. Kichenassamy, A. Kumar, P. Olver, A. Tannenbaum, and A. Yezzi, *Conformal curvature flows: From phase transitions to active vision*, Archive for Rational Mechanics and Analysis, **134** (1996), 275–301.
[10] A. Stuart and A.R. Humphries, *Dynamical system and numerical analysis*, Cambridge University Press, Cambridge, 1998.
[11] U. Trottenberg, C. Oosterlee, and A. Schüller, *Multigrid*, Academic Press, USA, 2001.
[12] L.A. Vese and T.F. Chan, *A multiphase level set framevork for image segmentation using the mumford and shah model*, International Journal of Computer Vision, **50** (3) (2002), 271–293.
[13] A. Yezzi Jr, S. Kichenassamy, A. Kumar, P. Olver, and A. Tannenbaum, *A geometric snake model for segmentation of medical imagery*, IEEE Transaction on Medical Image, **16** (2) (1997), 199-209.